Mitra Sadat Lavasani[1] / Rahbar Rahimi[1] / Mortaza Zivdar[1] / Mohammad Kalbassi[2]

# CFD Modeling to Predict Mass Transfer in Multicomponent Mixtures

[1] Department of Chemical Engineering, University of Sistan and Baluchestan, P.O. Box 98164–161 Zahedan, Iran (Islamic Republic of), E-mail: mit.lavasany@yahoo.com, rahimi@hamoon.usb.ac.ir, mzivdar@yahoo.com
[2] Brunel University London, Uxbridge UB8 3PH UK, E-mail: mohammad.kalbassi@brunel.ac.uk

**Abstract:**
A novel three-dimensional computational fluid dynamics mass transfer (CMT) model in Eulerian–Eulerian frame work is deploys for investigating the concentration profiles, and trays efficiencies in multicomponent distillation columns. The proposed model is based on Maxwell Stefan equations, and CFD was employed as a powerful tool to model the hydrodynamics and mass transfer. The two phases are modelled as two interpenetrating phases with interphase momentum, heat and mass transfer. The Closure model is developed for mass interphase transfer rate in ternary mixtures. The predictability of the mass transfer behaviours of multicomponent can result in a more efficient and predictable design of distillation trays. Two non-ideal ternary mixtures were studied. The tray geometry and operating conditions are based on the experimental works of Kalbassi and the composition profiles, tray efficiencies, and point efficiencies of mixtures were presented. The obtained results were confirmed by the experimental data. The results indicate that the values of individual component tray efficiencies and point efficiencies for these multicomponent systems were considerably different which confirm the interactive nature of the mass transfer in multicomponent mixtures. These mixtures also illustrated different point efficiencies across the tray because of the composition dependency of these mixtures. The average relative error for the prediction of efficiencies is about 8 %, which indicates the accuracy of the model.

**Keywords:** distillation, mass transfer, multicomponent, efficiency, CFD

## 1 Introduction

The sieve tray column is one of the widely word separation equipment in chemical and petrochemical industries. These columns are commonly applied in processes which involve the mass transfer between the liquid and vapor phases such as distillation and absorption. Although many researchers investigated the behavior of the sieve trays; the complex systematic interactive behaviors of flow and mass transfer inside the trays are not totally determined yet. One of these limitations is the prediction of the tray efficiency for binary and especially for multicomponent systems.

The mass transfer in trays is affected by the predominant hydrodynamics. Various attempts were made to study the behavior of the biphase on sieve trays [1, 2]. An enormous amount of research observed the stagnant zones and flow non-uniformities which reduce the efficiency of trays [3, 4]. A lot of attempts were made to investigate the hydrodynamics of trays by utilizing CFD [5–8]. Krishna et al. [9] employed a transient two-phase CFD model to simulate flow behaviors of a rectangular and circular tray. Fisher and Quarini [7] assumed a constant value of 0.44 for the drag coefficient. This value is appropriate for uniform Marangoni positive bubbly flow however; it is not the case for the froth flow regime in trays of distillation columns. Van Batten et al. [10] developed a drag coefficient relation which was independent of bubble size and is suitable for CFD simulation of distillation trays. This approach was utilized by many authors and was proved to be acceptable [11–13].

Rahimi et al. [14] were among the first researcher that developed a three dimensional two-fluid CFD model for predicting temperature and concentration distributions on sieve trays. They utilized Higbie mass transfer theory [15], and their tray geometries and operating conditions were based on the literature experimental data [16, 17]. The Higbie theory was extensively applied on CFD simulation of gas – liquid mass transfer in distillation columns even though its dependency on the bubble size is its drawback [12, 18, 19]. In addition, Rahimi et al. [20] used SRS mass transfer theory to study hydrodynamics, heat and mass transfer of sieve trays

Rahbar Rahimi is the corresponding author.
© 2019 Walter de Gruyter GmbH, Berlin/Boston.

by utilizing a 3D two-phase CFD model. It was perceived that SRS model is independent of the size of bubbles and so is more suitable for CFD simulation. This model was also applied by researchers to investigate the mass transfer performance on trays [21, 22]. Zhimin et al. [23] proposed a computational mass transfer model with distributed source term. The model is capable of predicting the concentration profile, the turbulent mass transfer diffusivity, and the Murphree efficiency of the sieve tray distillation column. Gesit [24] presented a CFD model to predict sieve tray hydrodynamics and mass transfer. He utilized Bennett et al. correlation [25] for predicting the Murphree and the point efficiency of distillation tray.

Although the multicomponent distillation is the dominant separation process of the chemical and petrochemical industries, there is very limited knowledge about the efficiencies of multicomponent mixtures as compared with the simpler case of binary mixtures. This lack of information resulted in designing multicomponent systems, based on the binary systems. The common assumption was that the behavior of multicomponent systems and binary systems is in the same manner [26]. This assumption is just true for thermodynamically ideal mixtures if the liquid mixing on tray would be complete whereas, in large trays with longer liquid flow paths which are used in industries, the partial liquid mixing exists [27]. The maldistribution of flow on the tray has a significant effect, not only on the overall tray efficiency but on the individual components as well. Biddulph [27] suggested the use of an eddy diffusion model to consider the extent of the liquid back mixing on the tray. It was reported that although all of the components have the same point efficiencies, the component tray efficiencies are different [28].

For non-ideal multicomponent mixtures, significant differences exist between binary and ternary mass transfer which aroused from the interactions between the diffusing species. These interactions were determined as: diffusion barrier, osmotic diffusion, and reverse diffusion. A considerable amount of research was studied about the mass transfer behavior of the non ideal mixtures, and they reported the differences between the individual component point efficiencies for ternary systems [29–34].

Efficiency data of ternary component distillation columns are less available than the data of binary distillation systems. As previously mentioned, in recent years, there has been growing attention paid to modeling mass transfer of binary mixtures using CFD simulation however; CFD modeling of multicomponent systems is so rare [35]. The lacking of in-depth perception of the mass transfer behaviors of multicomponent on the distillation trays is the main obstacle for the accurate prediction of tray efficiency and design. Therefore, it is crucial to develop a model for predicting the mass transfer behavior of multicomponent systems and an efficient evaluation.

The major purpose of the current study is to develop a CMT model to simulate the mass transfer of multicomponent mixtures inside a tray, to predict tray and point efficiencies. There has recently been considerable interest in simulating and designing the distillation column of multicomponent mixtures. Accordingly, a CFD model is needed to be able to simulate the multicomponent systems, and to improve our knowledge about the behavior of components in multicomponent mixtures. So, the intention is to predict individual component efficiencies in multicomponent systems. The results presented in the present paper are among the first attempt for investigating the behavior and concentration distributions of the multicomponent system using CFD and validating the model with the available experimental data [36]. Even though the experimental data are for a rectangular tray, the CFD model is capable to be adopted for a circular tray by changing the geometry as required in the CMT studies.

# 2 Computational fluid dynamic modeling

## 2.1 Hydrodynamic model

The model includes the two phase flow and mass transfer in the Eulerian − Eulerian framework, where both gas and liquid phases were treated as two interpenetrating phases with separate transport equations. The detail description of the multiphase flow transport equations are presented by Ranade [37]. The two-fluid conservation equations for two phase flow are as follows:

### 2.1.1 Continuity equations

Gas phase:

$$\frac{\partial}{\partial t}(\alpha_G\rho_G) + \nabla \cdot (\alpha_G\rho_G u_G) + S_{LG} = 0 \tag{1}$$

Liquid phase:

$$\frac{\partial}{\partial t}(\alpha_L \rho_L) + \nabla \cdot (\alpha_L \rho_L u_L) - S_{LG} = 0 \tag{2}$$

$S_{LG}$ is the interphase mass-transfer rate, and mass transfer between phases must satisfy the local balance condition:

$$S_{LG} = -S_{GL} \tag{3}$$

### 2.1.2 Momentum conservation

Gas phase:

$$\frac{\partial}{\partial t}(\alpha_G \rho_G u_G) + \nabla \cdot (\alpha_G(\rho_G u_G u_G)) = \nabla \cdot (\alpha_G \mu_{eff,G}(\nabla u_G + (\nabla u_G)^T)) - \alpha_G \nabla p_G + \alpha_G \rho_G g - M_{GL} \tag{4}$$

Liquid phase:

$$\frac{\partial}{\partial t}(\alpha_L \rho_L u_L) + \nabla \cdot (\alpha_L(\rho_L u_L u_L)) = \nabla \cdot (\alpha_L \mu_{eff,L}(\nabla u_L + (\nabla u_L)^T)) - \alpha_L \nabla p_L + \alpha_L \rho_L g + M_{GL} \tag{5}$$

The term $M_{GL}$ describes the interphase momentum transfer between the two phases and basically is the interphase drag force per unit volume. The equation for $M_{GL}$ is as below:

$$M_{GL} = \frac{3}{4}\frac{C_D}{d_G}\alpha_G \rho_L |u_G - u_L|(u_G - u_L) \tag{6}$$

$C_D$ is the drag coefficient and the drag correlation proposed by Van Batten et al. [10] has been used. The interphase momentum transfer term in a CFD suitable form is:

$$M_{GL} = \frac{(\alpha_G^{average})^2}{U_S^2}g(\rho_L - \rho_G)\alpha_G |u_G - u_L|(u_G - u_L) \tag{7}$$

Where, $\alpha_G^{average}$ is the average gas holdup fraction. Bennett et al. correlation [38] was considered:

$$\alpha_G^{average} = 1 - \exp[-12.55(U_S\sqrt{\frac{\rho_G}{\rho_L - \rho_G}})^{0.91}] \tag{8}$$

### 2.1.3 Volume conservation equation

The volume fractions of phases are related by the summation constraint:

$$\alpha_G + \alpha_L = 1 \tag{9}$$

### 2.1.4 Pressure constraint

Two phases are in equilibrium so share the same pressure field:

$$P_G = P_L \tag{10}$$

## 2.2  Mass transfer model

For the mass transfer, the transport equations for each spice are:
Gas phase:

$$\frac{\partial}{\partial t}(\alpha_G \rho_G y_i) + \nabla \cdot [\alpha_G(\rho_G u_G y_i - \rho_G D_{iG}(\nabla \cdot y_i))] - S_{LG} = 0 \tag{11}$$

Liquid phase:

$$\frac{\partial}{\partial t}(\alpha_L \rho_L X_i) + \nabla \cdot [\alpha_L(\rho_L u_L x_i - \rho_L D_{iL}(\nabla \cdot x_i))] + S_{LG} = 0 \tag{12}$$

The source term $S_{LG}$, is the interphase mass-transfer rate which is an important term in solving the mass transfer equations and affected highly on the final result.
The rate of local mass transfer $S_{LG}$ for binary mixture was expressed by [12]:

$$S_{LG} = K_{OG} a \rho_A (y_A - y_A{}^*) \tag{13}$$

The total molar flux in mixture with n component is obtained by [33]:

$$n_t = \sum_{i=1}^{n-1} n_i \tag{14}$$

Medina et.al [33] expressed the fluxes of components 1 and 2, in ternary system as:

$$n_1 = (K_{OG})_{11}(y_1^* - y_1) + (K_{OG})_{12}(y_2^* - y_2) \tag{15}$$

$$n_2 = (K_{OG})_{21}(y_1^* - y_1) + (K_{OG})_{22}(y_2^* - y_2) \tag{16}$$

So, the rate of local mass transfer for ternary mixture can be defined as:

$$S_{LG} = a M_A [(K_{OG})_{11}(y_1{}^* - y_1) + (K_{OG})_{12}(y_2{}^* - y_2) + (K_{OG})_{21}(y_1{}^* - y_1) + (K_{OG})_{22}(y_2{}^* - y_2)] \tag{17}$$

Where $(K_{OG})_{11}$, $(K_{OG})_{12}$, $(K_{OG})_{21}$, $(K_{OG})_{22}$ are the elements of the matrix of over-all gas-phase mass transfer coefficient $[K_{OG}]$. It is noteworthy that, the correlations by Zeiderweg [39] were used to estimate the effective vapor-liquid interfacial area.

### 2.2.1  Ternary overall gas phase mass transfer coefficient

The ternary overall gas phase mass transfer coefficient proposed by Krishna which consider the resistance in both phases, is used [40, 41]:

$$[K_{OG}]^{-1} = [K_G]^{-1} + [m][K_L]^{-1} \tag{18}$$

Where $[K_G]$ is the matrix of ternary gas phase mass transfer coefficients. Because of the complicated molecular interactions in the multicomponent mass transfer, the mass transfer rate strongly dependent on the composition. Therefore, the mass transfer coefficient is complex in a multicomponent system and may be estimated under the individual condition from the coefficients of relevant two-component pairs [11]. Diener and Gerster [31] expressed the ternary gas phase mass transfer coefficients, based on the gas phase mass transfer coefficients. So $K_G$ terms are a function of binary $k_G$ terms which are defined as:

$$(K_G)_{11} = [(1 - y_1)(k_G)_{12}(k_G)_{13} + (y_1)(k_G)_{13}(k_G)_{23}]/\phi \tag{19}$$

$$(K_G)_{12} = (y_1)(k_G)_{23}[(k_G)_{13} - (y_1)(k_G)_{12}]/\phi \tag{20}$$

$$(K_G)_{21} = (y_2)(k_G)_{13}[(k_G)_{23} - (k_G)_{12}]/\phi \tag{21}$$

$$(K_G)_{22} = [(1 - y_2)(k_G)_{12}(k_G)_{23} + (y_2)(k_G)_{13}(k_G)_{23}]/\phi \tag{22}$$

and

$$\phi = y_1(k_G)_{23} + y_2(k_G)_{13} + y_3(k_G)_{12} \tag{23}$$

Also $[K_L]$ is the matrix of ternary liquid phase mass transfer coefficients and $K_L$ terms are a function of binary $k_L$ terms. which are defined by substituting $(K_L)$ by $(K_G)$, and $(K_{Lij})$ by $(K_{Gij})$.

### 2.2.2   Binary mass transfer coefficients

The Higbie penetration theory [15] has been widely used to estimate the gas mass transfer coefficient in distillation [14]. Therefore the binary gas mass transfer coefficients are estimated by:

$$k_G = 2\sqrt{\frac{D_G}{\pi\theta_G}} \tag{24}$$

$D_G$ is gas phase diffusion coefficient which is presented as the binary gas diffusivities [36]. The contact time for gas in the froth region is:

$$\theta_G = \frac{d_B}{V_H} \tag{25}$$

Where $V_H$ is gas velocity through the tray holes, and $d_B$ is the bubble diameter that in one approach can assume to be equal to mean diameter of bubbles [12] and also $d_B$ can be estimated with the relation for bubble diameter given by Bennett et al. [25]. This equation has been used previously by Gesit [24]:

$$d_B = \left(\frac{-12/\sqrt{\pi}}{1 + m\frac{\rho_{MV}}{\rho_{ML}}\sqrt{\frac{V_H D_G}{V_{Rise} D_L}}}\frac{h_F\sqrt{V_H D_G}}{V_{Rise}\ln(1 - E_{OV})}\right)^{2/3} \tag{26}$$

$$E_{OV} = 1 - \exp\left[\frac{-0.0029}{1 + m\frac{\rho_{MV}}{\rho_{ML}}\sqrt{\frac{r_G^{average}D_G}{D_L(\frac{A_H}{A_B})}}}\left(\frac{\rho_G V_H h_F}{\mu_G}\right)^{0.4136}\left(\frac{h_L}{d_h}\right)^{0.6074}\left(\frac{A_H}{A_B}\right)^{-0.3195}\right] \tag{27}$$

Where the clear liquid height $h_L$ was estimated by [38]:

$$h_L = \alpha\left[h_w + c\left(\frac{Q_L}{\alpha L_W}\right)^{2/3}\right] \tag{28}$$

With $\alpha = 1 - r_G^{average}$ and $c = 0.501 + 0.439\exp(-137.8h_w)$.

    Furthermore, the SRS theory [42] was applied to approximate the liquid mass transfer coefficient. The SRS model consists of both turbulent and convective mass transfer at the gas–liquid interface. Moreover, the SRS model diminishes the dependency of the simulation results to the bubble diameters. The SRS mass transfer coefficient used by Rahimi et al. is [20]:

$$k_L = 2\left(\frac{D_L}{\pi}\sqrt{\frac{U_{sg}g}{\kappa}}\right)^{1/2} \tag{29}$$

In the liquid phase, the "Eddy diffusion" model of Bennett et al. [43] was used instead of the molecular diffusivity to consider the extent of the liquid back mixing in simulations.

### 2.2.3 Slope of equilibrium line

The $[m]$ in eq. (18) is the matrix of coefficients for the linearized relationship [38]:

$$m_{ij} = \frac{\partial y_i}{\partial x_j}, i, j = 1, 2, \dots n - 1 \tag{30}$$

For equilibrium between two phases which have the same temperature and pressure the equation of fugacity for any component i, in either phase is:

$$\phi_i y_i P = \gamma_i x_i P_i^s, i = 1, 2, \dots, n \tag{31}$$

From eqs. (35) and (36) obtained:

$$\begin{aligned} m_{ij} = \frac{\partial y_i}{\partial x_j} &= \frac{\partial(\gamma_i x_i)}{\partial x_j} \frac{P_i^s}{\phi_i P} \\ &= x_i \frac{\partial \ln(\gamma_i x_i)}{\partial x_j} \frac{\gamma_i P_i^s}{\phi_i P} = \Gamma_{ij} K_{eqi}, i, j = 1, 2, \dots, n - 1 \end{aligned} \tag{32}$$

Where the $\Gamma_{ij}$ s are thermodynamic correction factors (activity coefficient) and calculated as [11]:

$$\Gamma_{ij} = \delta_{ij} + \frac{x_i}{x_j} \cdot \frac{\partial \ln \gamma_i}{\partial \ln x_j}, i, j = 1, 2, \dots, n - 1 \tag{33}$$

By substituting eq. (37) in eq. (18):

$$[K_{OG}]^{-1} = [K_G]^{-1} + \langle K_{eq} \rangle [\Gamma] [K_L]^{-1} \tag{34}$$

In addition, the ternary equilibrium relationships are evaluated in the following form [32]:

$$y_1^* = m_{11} x_1 + m_{12} x_2 \qquad , \qquad y_2^* = m_{21} x_1 + m_{22} x_2 \tag{35}$$

Where the slope of the equilibrium lines ($m_{ij}$) are calculated from eq. (37). In CFD simulation for each two component, the mass transfer coefficients and slope of equilibrium lines are defined separately. It is important to notice that, although the fluxes calculated in the ANSYS CFD code should be expressed on a scalar basis, matrix calculations were performed and the appropriate form was used in the simulations.

## 3 Model flow geometry and the experiment conditions

The experimental equipment used here has been described previously by Rahimi et al. [12, 20]. They utilized this rectangular sieve tray for the investigation of binary mass transfer. The experimental data which used in this study are presented by Kalbassi [36]. All the experiments were done at atmospheric pressure and at the total reflux, and were carried out at a superficial F-Factor of about 0.5 (Pa)$^{0.5}$. Schematic of test tray is demonstrated in Figure 1. The detail of the simulated tray is presented in Table 1. Wilson's equations are applied in present simulations for estimating the mixture activity coefficient. The equilibrium data of the systems in the form of the thermodynamically consistent Wilson parameters were used as reported in Table 2 [36]. All these VLE data presented in Kalbassi thesis [36]. In addition, the physical properties of components are given by Kalbassi.
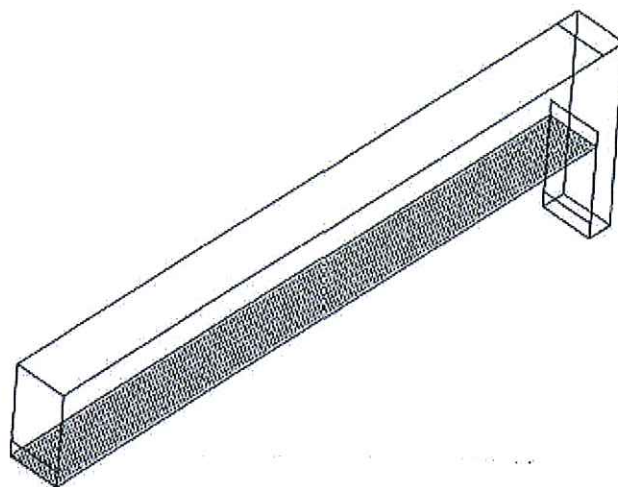
**Figure 1:** Geometry of simulated rectangular sieve tray.

**Table 1:** Tray specifications [44].

| Weir length | 83 mm |
|---|---|
| Liquid flow-path length | 991 mm |
| Tray spacing | 154 mm |
| Hole diameter | 1.8 mm |
| Triangle hole pitch | 6.1 mm |
| No. of holes | 2586 |
| % Free area | 8 |
| Outlet weir height | 25 mm |
| Inlet weir height | 4.8 mm |

**Table 2:** Binary Wilson parameters [36].

| System | Wilson parameter |
|---|---|
| Methanol-n.propanol | 421.821, −245.905 |
| Methanol-water | 216.851, 468.601 |
| Ethanol-water | 216.756, 975.488 |
| n.propanol-water | 906.526, 13969.639 |

In simulations, the following boundary conditions are applied. Uniform liquid inlet velocity and constant mole fraction values for entering liquid phase were specified. Inlet gas flow rate was defined. The gas volume fraction at the inlet was specified to be unity. The liquid and gas outlet boundaries were defined as mass flow boundary conditions. A no-slip wall boundary condition was used for the liquid phase and a free slip wall boundary condition was specified for the gas phase.

It is well known that the number of meshes has a significant effect on the convergence and accuracy of the results. For these simulations, unstructured tetrahedral meshes were applied using ICEM CFD. Different mesh sizes were selected for different positions of the computational domain. Finer meshes were adopted above and below the tray, which is the main region of gas and liquid contact. Moreover, meshes were refined adjacent to the holes in order to ensure the accuracy at interfaces. The grid independency study for the case of WF was investigated was carried out to determine the effect of grid size on the calculated results as shown in Table 3. The grid convergence requires that after a certain grid number the numerical results do not change significantly as number of grids is further increases. As it is shown in Table 3, by increasing the number of nodes, the estimated froth height by CFD became slightly better. After the determined number of nodes the results did not did not change significantly. Accordingly, for lowering computational effort, the simulations were performed with 986,803 nodes.

**Table 3:** Grid independency study.

| Number of nodes | Froth height (m) |
|---|---|
| 253,823 | 0.073754 |
| 399,257 | 0.072541 |
| 610,994 | 0.072185 |
| 986,803 | 0.072059 |
| 1,197,312 | 0.072061 |
| 1,469,596 | 0.072060 |

# 4 Simulation results and discussion

## 4.1 Tray hydrodynamics

Two highly non ideal ternary mixtures (MeOH/n.PrOH/H2O, MeOH/EtOH/H2O) were utilized for simulation by CFD. Table 4 indicates the mean composition of each component and froth height which was presented by Kalbassi [36]. Table 4 also gives the froth heights from simulation results to compare these results with the experimental data. The simulated and experimental froth heights at each run are in a close agreement (with an average relative absolute value error of 5.32 %). Froth height is the key hydraulic parameter and was applied for validation of the hydrodynamics of the model. The froth height is expected to be a function of the vapor velocity and the liquid hold up on the tray [36].

**Table 4:** Average composition and froth heights.

| Run NO. | $\bar{X}$ | | | | Froth height (cm) | |
|---|---|---|---|---|---|---|
| | MeOH | n.PrOH | EtOH | $H_2O$ | Experimental data [36] | Simulated |
| WA | 0.1533 | 0.5213 | 0 | 0.3255 | 4.0 | 4.4 |
| WF | 0.0785 | 0.1343 | 0 | 0.7870 | 7.0 | 7.2 |
| XD | 0.4108 | 0 | 0.2193 | 0.3699 | 8 | 8.25 |

In addition, the horizontal liquid velocity values versus dimensionless width of tray, Z/W, is shown in Figure 2 for cases of WF and XD. The velocity distributions across the tray were not given by Kalbassi [36], thus no comparison between simulated and experimental data can be done. The trend of U velocity variation is similar to rectangular tray of Rahimi et al. [12, 20] and confirms the validity of the simulation results and the results shown that the mixture along the tray behaved closer to plug flow.
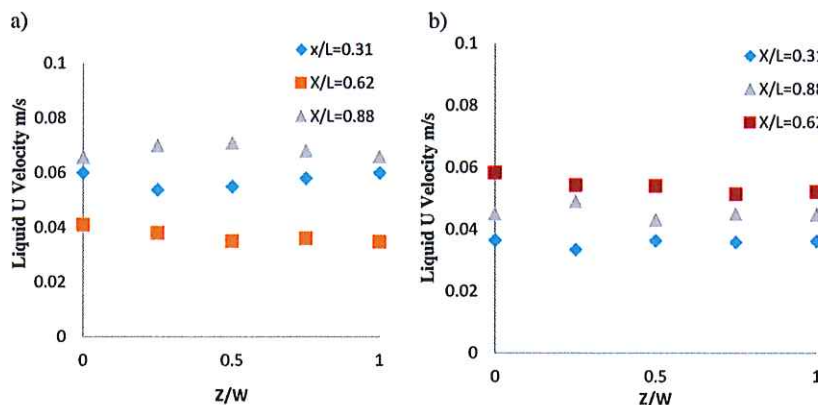


**Figure 2:** Liquid U-velocity profile across the tray for a) WF, b) XD.

## 4.2 Compositions profiles

Kalbassi [36] indicated the mean liquid concentration profiles of each component, for each case at total reflux condition. Also, he presented the Composition profile across the rectangular for the system

MeOH/n.PrOH/H$_2$0, which are predicted by the use of Krishna method [40]. The concentration profiles of each component resulted from the simulation were compared against the experimental data. Figure 3–Figure 5 illustrate the composition profiles from inlet (With "0" specified in Figure) to outlet (With "7" specified in Figure) of the tray. Furthermore, Figures included the CFD result the aid of Bennett et al. [38] correlation for predicting the bubble diameter in Higbie theory. These graphs were used for validation of mass transfer model. The Comparison indicated that the CFD simulation results are in the same trend by experimental data and are especially in a closed agreement by Krishna [40] model. This may be due to the use of Krishna model in CFD simulation which is the sign of a proper performance of the CFD model. The mean average error is about 0.03. Moreover, Bennett et al. [38] model slightly illustrated a tendency toward the values above or below the experimental results. However, the simulation results are in general agreement and in a proper trend with the experimental data. Comparison showed that the CFD simulation results and experimental data differ by an average of about 12 %. One possible reason for the mentioned deviation is the fact that Bennett et al. correlation [38] considers the liquid-continuous region as the region of mass transfer occurrence. Gesit [24] has also reported deviation in his results and stated that all simulations have a value of discrepancy which is acceptable.
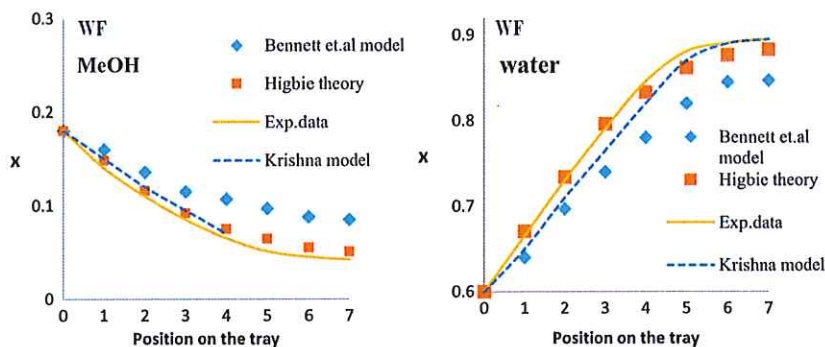


Figure 3: Liquid composition profiles of the ternary MeOH/n.PrOH/H$_2$0 across the tray for WF.
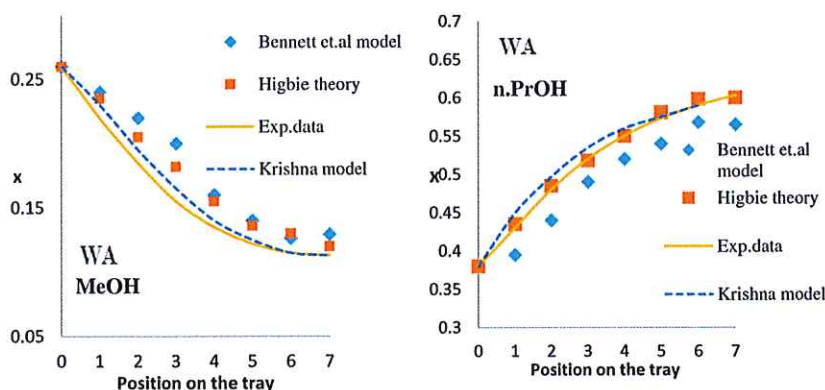


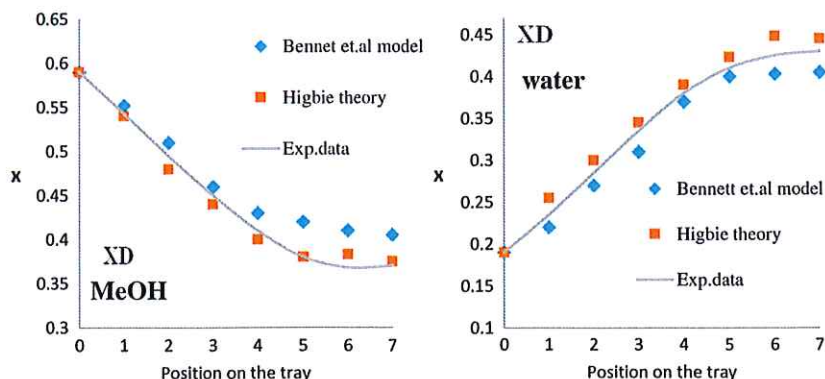Figure 4: Liquid composition profiles of the ternary MeOH/n.PrOH/H$_2$0 across the tray for WA.



Figure 5: Liquid composition profiles of MeOH/EtOH/H$_2$0 system across the tray for XD.

Figure 6 illustrates contour of water in vapor phase for the case of WA. The CFD results are in a good agreement with the experimental data. As previously mentioned, the experiments were carried out at total reflux, so the liquid compositions and vapor compositions are interdependent according to the equation $y_n = x_{n+1}$.

The obtained results are in closed agreement with this equation and confirmed the model utilized in these simulations.
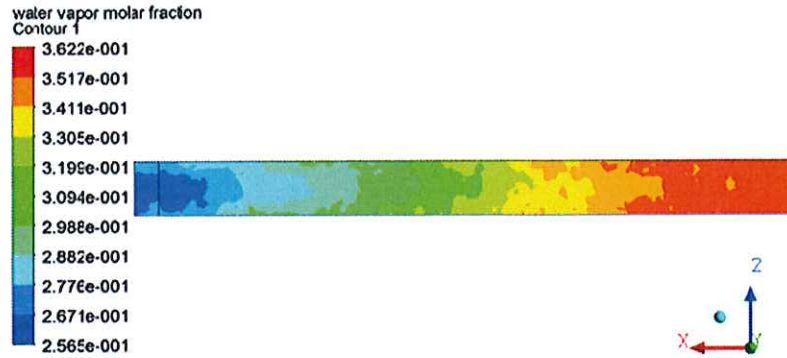


**Figure 6:** Snapshots of the top view of vapor phase water molar fraction for WA at z = 0.58 m.

## 4.3  Tray efficiency

The Murphree tray efficiency is based on a semi-theoretical model which related the theoretical number of stages with the actual trays in a distillation. It is the most common definition of tray efficiency in tray investigation and is defined as follows:

$$E_{MV} = \frac{y_n - y_{n-1}}{y_n^* - y_{n-1}} \tag{36}$$

Whereas the column operated at total reflux, $y_{n-1} = x_n$ so the eq. (36) can be written as:

$$E_{MV} = \frac{y_n - x_n}{y_n^* - x_n} \tag{37}$$

In addition to the experimental data, Kalbassi [36] has presented the tray efficiencies for each component which are predicted by the Eddy diffusion model. These efficiencies, together with the CFD tray efficiencies of the individual components for each run are included in Table 5. By comparing the tray efficiencies in Table 5, it is founded that the CFD predictions agree to the experimental data, especially by the predicted data from the model, with an average relative absolute value error of 7.77 %. This agreement is due to the use of eddy diffusion in the CFD model and confirms the exact prediction of the simulations. Furthermore, the Bennett et al. model [38] predicted the higher or, the lower tray efficiencies than the experimental data. This is probably the result of ignoring the impact of vapor-continuous region on the mass transfer model. However, this amount of error in the simulation is acceptable.

**Table 5:** Experimental data and CFD results for Murphree tray efficiency.

| Run | MeOH | | | | n.PrOH/EtOH | | | | water | | | |
|---|---|---|---|---|---|---|---|---|---|---|---|---|
| | Kalbassi [34] | | CFD | | Kalbassi [36] | | CFD | | Kalbassi [36] | | CFD | |
| | Exp | model | Higbie | Bennett | Exp | model | Higbie | Bennett | Exp | model | Higbie | Bennett |
| WF | 1.5 | 1.51 | 1.52 | 1.46 | 0.77 | 0.86 | 0.845 | 0.83 | 0.98 | 1.05 | 1 | 1.08 |
| WA | 1.22 | 1.28 | 1.3 | 1.19 | 1.16 | 1.33 | 1.3 | 1.28 | 1.73 | 1.42 | 1.39 | 1.35 |
| XD | 1.244 | 1.263 | 1.248 | 1.23 | 0.026 | 0.19 | 0.23 | 0.26 | 1.15 | 1.174 | 1.08 | 0.99 |

As expected, the individual components of these multicomponent systems were indicated to exhibit different tray efficiencies. One of the reasons could be the limited back mixing on the tray which affected on the individual component composition gradient across the tray. The other reason could be due to the thermodynamic non-idealities or effects of diffusion interactions which were formed in multicomponent systems from the presence of reverse diffusion, osmotic diffusion, or diffusion barrier effects [27, 29, 33]. Moreover, in multicomponent systems, individual components have different effective equilibrium line slopes that caused the different individual component tray efficiencies [28].

## 4.4   Point efficiency

An attempt was also made to predict the point efficiencies from CFD results. The Murphree point efficiency was calculated for the individual components as follows:

$$E_{og} = \frac{y_n - y_{n-1}}{y_n^* - y_{n-1}} \tag{38}$$

Where $y_{n-1}$, is the vapor inlet and $y_n$, is the vapor outlet (mol fraction). The contour of methanol point efficiencies for the case of WF is demonstrated in Figure 7. The point efficiency is composition dependent so it represents different point efficiencies at different points across the tray. The individual component point efficiencies demonstrated similar variations in point efficiencies for WF, and similar results are also reported by Kalbassi [36].
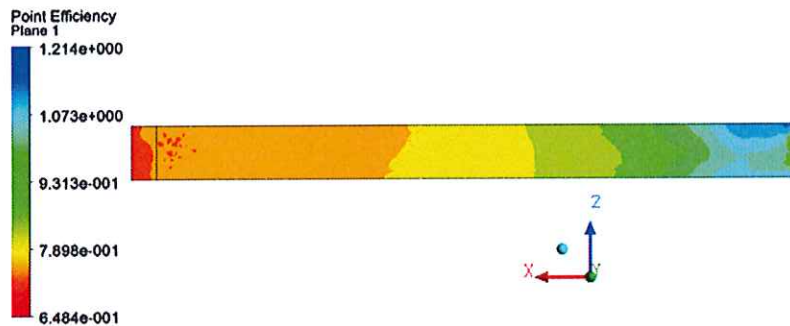


**Figure 7:** Snapshots of the top view of Point efficiency distribution.

The point efficiencies calculated for runs WA and XD are represented in Table 6. The experimental point efficiencies for individual components are included in Table 6. Kalbassi utilized the average composition on the tray to calculate point efficiencies. The individual component point efficiencies for these runs were founded to be different from each other. These differences in component point efficiencies are again related to large differences between the diffusion coefficients of the individual components [33] and in addition, individual components have different effective equilibrium line slopes which terminate the different individual component point efficiencies [28].

**Table 6:** experimental data and CFD results for Murphree point efficiency.

| Run | MeOH | | | water | | |
|-----|-----------|-------|--------|-----------|------|--------|
|     | Exp. data | CFD   | %Error | Exp. data | CFD  | %Error |
| WA  | 0.84      | 0.88  | 4.76   | 0.62      | 0.7  | 12     |
| XD  | 0.86      | 0.899 | 4.53   | 1.02      | 1.09 | 6.8    |

## 5   Conclusion

A 3-D two phase CFD model was developed for simulating the hydrodynamics and mass transfer performance of multicomponent systems. The proposed novel model, which is suitable for multicomponent CFD simulation, is based on Maxwell Stefan equations. The method expressed the ternary over all gas phase mass transfer

coefficients in terms of binary over all gas phase mass transfer coefficients. Two non ideal ternary mixtures were studied by employing the presented model. The tray geometries and operating conditions are based on the experimental data of Kalbassi [36]. The hydraulics parameters such as froth height and velocity distributions were measured. The composition profiles were determined across the tray by the aid of two methods. The Murphree point efficiencies and tray efficiencies were predicted by CFD. The obtained results were in good agreement with the experimental data. As expected, significant differences in individual component Murphree tray efficiencies were obtained even when equal component point efficiencies exhibited across the tray. These differences are due to none ideal and surface tension related interaction effects. Also, the point efficiencies were related to composition. The current study revealed that CFD modeling can be used as a powerful method to evaluate the multicomponent mixtures performance on distillation trays. Also, by means of CFD simulations, the efficiencies of the tray can be predicted which resulted in efficient design of distillation columns.

## Acknowledgments

## Nomenclature

$a$  effective interfacial area per unit volume, $m^{-1}$

$a^{/}$  interfacial area per unit bubbling area

$A_B$  tray bubbling area, $m^2$

$A_H$  area of holes, $m^2$

$b$  weir length per unit bubbling area, $m^{-1}$

$C_D$  drag coefficient, dimensionless

$d_B$  bubble diameter, m

$d_G$  the diameter of gas bubble, m

$d_h$  hole diameter, m

$D_G$  Gas molecular diffusivity, $m^2/s$

$D_L$  liquid molecular diffusivity, $m^2/s$

$E_{OV}$  vapor phase Murphree point efficiency

$F$  Fraction hole area per unit bubbling area

$F_{bba}$  vapor F-factor on bubbling area, $(m/s)(kg/m^3)^{0.5}$

$FP$  flow parameter

$g$  acceleration due to gravity, $9.81\,m/s^2$

$G_M$  molar gas rate per unit of bubbling area, $kmoles/hr.\,m^2$

$h_f$  froth height, m

$h_L$  clear liquid height, m

$h_W$  weir height, m

$k_G$  binary over all gas phase mass transfer coefficient, m/s

$K_G$  ternary over all gas phase mass transfer coefficient, m/s

$k_L$  liquid phase mass transfer coefficient, m/s

$Lw$  weir length, m

$m$  slope of equilibrium line

$M_{GL}$  interphase momentum transfer, $N/m^3$

$p$  pitch of holes in sieve plate, m

$P$  pressure ($N/m^2$)

$Q_L$ liquid volumetric flow rate, $m^3/s$

$S_{LG}$ rate of inter phase mass transfer, $kg/m^3s$

t Time, s

u velocity vector, $m/s$

$U_L$ time average liquid velocity on bubbling area, m.s

Us time average superficial vapor velocity, $m.s^{-1}$

$V_{slip}$ slip velocity between gas and liquid, $m/s$

$V_H$ hole velocity, $m/s$

x mass fraction in liquid phase, dimensionless

y mass fraction in gas phase, dimensionless

**Greek letters**

$\mu$ the viscosity of phase, Pa.s

$\rho$ the density of phases, $kg/m^3$

$\theta_G$ contact time in the gas phase, s

k kinematic viscosity, $m^2/s$

**Subscripts**

Eff Effective

G referring to gas phase

L referring to liquid phase

# References

[1] Smith BD. Design of equilibrium stage processes, 2nd ed. US: McGraw-Hill Companies, 1963 .

[2] Lockett MJ. Distillation tray fundamentals. Cambridge: Cambridge University Press, 1986 .

[3] Lockett MJ, Lim CT, Porter KE. The effect of liquid channelling on distillation column efficiency in the absence of vapour mixing. Trans Inst Chem Engrs. 1973;51:61.

[4] Bell RL. Residence time and fluid mixing on commercial scale sieve trays. AIChE J. 1972;18:498–505.

[5] Gesit G, Nandakumar K, Chuang KT. CFD modeling of flow patterns and hydraulics of commercial scale sieve trays. AIChE J. 2003;49:910–24.

[6] Rahimi MR, Karimi H. CFD simulation of hydraulics of sieve trays with gas mal-distribution. Chem Prod Process Model. 2010;5:Article 2. DOI: 10.2202/1934-2659.1252

[7] Fischer CH, Quarini GL. Three-dimensional heterogeneous modeling of distillation tray hydraulics. In: AIChE annual meeting. 15 Nov 1998:15–20.

[8] Lavasani MS, Rahimi R, Zivdar M. Hydrodynamic study of different configurations of sieve trays for a dividing wall column by using experimental and CFD methods. Chem Eng Process-Process Intensif. 2018;129:162–70.

[9] Krishna R, Van Baten JM, Ellenberger J, Higler AP, Taylor R. CFD simulations of sieve tray hydrodynamics. Trans IChemE. 1999;77:639–46.

[10] Van Baten JM, Krishna R. Modelling sieve tray hydraulics using computational fluid dynamics. Chem Eng J. 2000;77:143–51.

[11] Yu KT, Yuan X. Introduction to computational mass transfer. Heidelberg: Springer, 2014

[12] Rahimi R, Rahimi MR, Zivdar M. Efficiencies of sieve tray distillation columns by CFD simulation. Chem Eng Technol Ind Chem Plant Equip Process Eng Biotechnol. 2006;29:326–35.

[13] Liew SY, Gimbun J. CFD simulation on the hydrodynamics in gas-liquid airlift reactor. Chem Prod Process Model. 2017;12:20170030. DOI: 10.1515/cppm-2017-0030

[14] Rahimi MR, Rahimi R, Shahraki F, Zivdar M. Prediction of Temperature and Concentration Distributions of Distillation Sieve Trays by CFD. Journal of Applied Science and Engineering. 2006;9:265–78. Journal name was "Tamkang Journal of Science and Engineering" before 2012.

[15] Higbie R. The rate of absorption of a pure gas into a still liquid during short periods of exposure. Trans AIChE. 1935;31:365–89.

[16] Dribika MM, Biddulph MW. Scaling up distillation efficiencies. AIChE J. 1986;32:1864–75.

[17] Yanagi T, Sakata M. Performance of a commercial scale 14% hole area sieve tray. Ind Eng Chem Process Des Dev. 1982;21:712–7.

[18] Jiang B, Liu P, Zhang L, Sun Y, Wang H, Liu Y, et al. Hydrodynamics and mass-transfer analysis of a distillation ripple tray by computational fluid dynamics simulation. Ind Eng Chem Res. 2013;52:17618–26.

[19] Rahimi MR. A combined computational fluid dynamics and artificial neural networks model for distillation point efficiency. Chem Prod Process Model. 2012;7:Article 5. DOI: 10.1515/1934-2659.1636

[20] Rahimi R, Sotoodeh MM, Bahramifar E. The effect of tray geometry on the sieve tray efficiency. Chem Eng Sci. 2012;76:90–8.

[21] Zhang L, Li Z, Yang N, Jiang B, Pavlenko AN, Volodin OA. Hydrodynamics and mass-transfer characteristics analysis of vapor–liquid flow of dual-flow tray. J Eng Thermophys. 2016;25:449–63.

[22] Zhang L, Li Z, Yang N, Jiang B, Cong H, Zhang Z. Hydrodynamics and mass transfer performance of vapor–liquid flow of orthogonal wave tray column. J Taiwan Inst Chem Eng. 2016;63:6–16.

[23] Zhimin SU, Chunjiang LI, Guocong YU, Xigang YU. Prediction of distillation column performance by computational mass transfer method. Chin J Chem Eng. 2011;19:833–44.

[24] Gesit G. Sieve tray efficiency using CFD modeling and simulation. Zede J. 2013;30:1–6.

[25] Bennett DL, Watson DN, Wiescinski MA. New correlation for sieve tray point efficiency, entrainmnt, and section efficiency. AIChE J. 1997;43:1611–26.

[26] Biddulph MW, Kalbassi MA, Dribika MM. Multicomponent efficiencies in two types of distillation column. AIChE J. 1988;34:618–25.

[27] Biddulph MW. Multicomponent distillation simulation—distillation of air. AIChE J. 1975;21:327–35.

[28] Toor HL. Diffusion in three-component gas mixtures. AIChE J. 1957;3:198–207.

[29] Toor HL, Burchard JK. Plate efficiencies in multicomponent distillation. AIChE J. 1960;6:202–6.

[30] Krishna R, Wesselingh JA. The Maxwell-Stefan approach to mass transfer. Chem Eng Sci. 1997;52:861–911.

[31] Diener DA, Gerster JA. Point efficiencies in distillation of acetone-methanol-water. Ind Eng Chem Process Des Dev. 1968;7:339–45.

[32] Krishna R, Standart GL. Mass and energy transfer in multicomponent systems. Chem Eng Commun. 1979;3:201–75.

[33] Medina AG, McDermott TC, Ashton N. Prediction of multicomponent distillation efficiencies. Chem Eng Sci. 1979;34:861–6.

[34] Krishna R, Martinez HF, Sreedhar R, Standart GL. Murphree point efficiencies in multicomponent systems. Trans Inst Chem Engrs. 1977;55:178.

[35] Padoin N, Dal'Toé AT, Rangel LP, Ropelato K, Soares C. Heat and mass transfer modeling for multicomponent multiphase flow with CFD. Int J Heat Mass Transf. 2014;73:239–49.

[36] Kalbassi MA. Distillation sieve tray efficiencies. Doctoral dissertation, University of Nottingham, 1987.

[37] Ranade VV. Computational flow modeling for chemical reactor engineering. NY: AP, 2001

[38] Bennett DL, Agrawal R, Cook PJ. New pressure drop correlation for sieve tray distillation columns. AIChE J. 1983;29:434–42.

[39] Zuiderweg FJ. Sieve trays: a view on the state of the art. Chem Eng Sci. 1982;37:1441–64.

[40] KRISHNA R. A simplified film model description of multicomponent interphase mass transfer. Chem Eng Commun. 1979;3:29–39.

[41] Krishna R. Prediction of multicomponent distillation efficiencies. Chem Eng Sci. 1980;35:2371.

[42] Jajuee B, Margaritis A, Karamanev D, Bergougnou MA. Application of surface-renewal-stretch model for interface mass transfer. Chem Eng Sci. 2006;61:3917–29.

[43] Bennett DL, Grimm H. Eddy diffusivity for distillation sieve trays. AIChE J. 1991;37:589–96.

[44] Biddulph MW, Kalbassi MA. Distillation efficiencies for methanol/1-propanol/water. Ind Eng Chem Res. 1988;27:2127–35.